

Metallic to insulating nature of TaN_x: Role of Ta and N vacancies

C. Stampfl and A. J. Freeman

Department of Physics and Astronomy, Northwestern University, Evanston, Illinois 60208-3112

(Received 24 June 2002; revised manuscript received 2 October 2002; published 28 February 2003)

It has been demonstrated recently that the stoichiometry of rocksalt TaN can be tuned by N₂ pressure and temperature, yielding material that ranges from highly conductive to insulating. Using density functional theory, we investigate the atomic and electronic structure and formation energy of defective TaN structures. The calculations predict that Ta and N vacancies form under N-rich and N-poor conditions, respectively, where the presence of Ta vacancies reduce the density of states (DOS) around the Fermi level (E_F). We also studied the Ta₄N₅ and Ta₃N₅ structures which occur in nature. The former phase, consisting of an ordered arrangement of Ta vacancies, also exhibits a notable decrease in the DOS at E_F , while the latter is a semiconductor with a band gap of 1.5 eV within the local density approximation. Our results suggest that the formation of Ta-deficient structures is directly related to the metal-to-insulator transition.

DOI: 10.1103/PhysRevB.67.064108

PACS number(s): 71.30.+h, 68.35.Dv

I. INTRODUCTION

Current interest in tantalum nitride is related to its possible use as an electronic material. In particular, the performance of semiconductor devices in terms of component density and speed is predicted to be limited by the extra power that the device would require in order to reach higher speeds. Thus, alternative technologies are being pursued, one of which, rapid-single-flux-quantum (RSFQ) logic, is based on superconductors and holds promise for the highest speeds in digital electronics.¹ Pulses can be sent at close to the speed of light, and Josephson junctions provide switching in the picosecond regime and use only millivolts (instead of a few volts)—and thus require and dissipate very little power. A drawback is that they must operate at very low temperatures, e.g., at 4–5 K for Nb-based devices. Because of this potential application, there is strong interest in superconductor/normal-conductor/superconductor (SNS) junctions. For these systems, the figure of merit is the product of the current and resistivity, IR , since it is proportional to the SFQ pulse. For example, for 50 GHz operation, one requires $IR > 320 \mu\text{V}$. This is significantly higher than the maximum clock frequency of ≈ 0.3 GHz in 1997, which was predicted to reach just 1.1 GHz in 2010 on the basis of current technologies.¹

Recent experiments have shown that the NbN/TaN_x/NbN system exhibits desired parameters for RSFQ circuitry² when the barrier material TaN_x has a resistivity close to the metal-insulator transition. The resistivity can be tuned by the growth conditions, namely, by the nitrogen pressure and the temperature.^{2–5} For example, the stoichiometry (properties) can be varied from Ta_{1.12}N (metallic) to Ta_{0.90}N (metallic) to Ta_{0.74}N (barely metallic) to Ta_{0.66}N (insulating), by increasing the N₂ pressure. X-ray diffraction experiments indicate that the (metastable) rocksalt structure is essentially maintained.^{3,6} Thus, the local atomic geometries in these nonstoichiometric structures likely involve native defects. Tantalum nitride was also found to be a promising material for other applications, such as diffusion barriers in copper interconnects on Si chips⁷ and to make compact thin-film resistors. The Ta-N system is relatively unexplored and, unlike, e.g., the Ti-N system, it exhibits a remarkable richness

in the array of equilibrium and metastable phases that can form;⁸ indeed more than 11 have been reported, where very little is known about their relative stability.

In this paper, we investigate the atomic and electronic structure and formation energies of defective TaN structures in order to gain insight into the mechanism giving rise to the variation in conductivity. We focus in particular on N-rich structures which are found to have dramatically increased resistivities compared to stoichiometric rocksalt TaN.⁹ For comparison, we also perform calculations for two other phases which form in nature and which also have N-rich stoichiometries, namely, Ta₄N₅ (Ref. 10) (a defective rocksalt structure) and Ta₃N₅ (Ref. 11) (an orthorhombic structure). Based on the calculated energetics and electronic structures, our results point to Ta vacancies as being largely responsible for the metallic-to-insulating transition. This prediction is consistent with indications from early work that higher nitrides of Ti, Zr, and Hf involve metal vacancies, on the basis of experiments (Ti, Zr, Hf) (Ref. 12) and theory (Zr) (Ref. 13). Investigations of the electronic properties of refractory compounds of transition-metal nitrides and carbides containing typical structural defects such as vacancies, interstitial, and substitutional impurities have been reported;¹⁴ to our knowledge, however, there have been no such studies for TaN. Some results that were briefly reported in Ref. 3 are presented in detail here.

II. CALCULATION METHOD

The density functional theory (DFT) calculations are performed using the first-principles full-potential linearized augmented-plane-wave (FLAPW) method¹⁵ and in its parallelized form¹⁶ with the local density approximation¹⁷ (LDA) for the exchange-correlation functional. We treat the core states fully relativistically and the valence states scalar relativistically, and use angular momenta up to $l=8$ in the muffin-tin spheres for both the wave functions and charge density in the self-consistent cycles. We consider high and low defect concentrations by using 8- and 32-atom cells to model the defect systems. For the former, the energy cutoff for the plane-wave expansion in the interstitial region be-

tween the muffin-tin spheres is taken to be 25 Ry, and also for the 18-atom Ta₄N₅ structure. For the larger 32-atom systems, which include the Ta₃N₅ structure, a slightly lower (but still high) cutoff of 20.7 Ry was used. Thirty-five **k** points are taken in the irreducible part of the Brillouin zone (IBZ) for the “8-atom” cells and 27 for the Ta₄N₅ structure.¹⁸ For the larger 32-atom cells, we used (2×2×2) (defect cells) and (4×4×4) (Ta₃N₅ phase) Monkhorst-Pack grids.¹⁸ The muffin-tin radii R_{MT} for all calculations are $R_{\text{N}}=1.4$ bohr for the N atom and $R_{\text{Ta}}=2.47$ bohrs for the Ta atom, with the exception of the N interstitial, for which we used $R_{\text{Ta}}=2.10$ bohrs, due to the closer Ta-N distances caused by the interstitial N atom, and $R_{\text{Ta}}=2.2$ bohrs for Ta₃N₅, also due to the closer N-Ta distance. Clearly, in the calculation of *energy differences*, as is required in obtaining the formation energies [cf. Eq. (1)], we take care to use exactly the same plane-wave cutoff, **k** points, and muffin-tin radii. The atomic positions of all atoms are fully relaxed until the force on each atom is less than 1 mRy/a.u.

To compare the relative stabilities of the various structures, we define the formation energy as¹⁹

$$E^f = (E_{\text{defect}}^{\text{tot}} - nE_{\text{Ta-bulk}}^{\text{tot}} - m/2E_{\text{N}_2}^{\text{tot}})/(m+n), \quad (1)$$

where $E_{\text{defect}}^{\text{tot}}$, $E_{\text{Ta-bulk}}^{\text{tot}}$, and $E_{\text{N}_2}^{\text{tot}}$ are the total energies of the Ta-N system calculated using the supercell, a bulk (bcc) Ta atom, and a free N₂ molecule, respectively; n and m are the number of Ta and N atoms in the supercell. E^f is, by definition, the heat of formation per atom of the structure under consideration.

Since in the experiments^{2,3} the stoichiometry was shown to depend sensitively on the nitrogen atmosphere, we take this effect into account as follows: We consider the system in contact with a nitrogen gas phase which is described by a pressure p and temperature T . The environment then acts as a reservoir, as it can give (or take) nitrogen atoms to (or from) the system without changing the temperature or pressure. We therefore calculate

$$E^f(\mu_{\text{N}}) \approx [E_{\text{defect}}^{\text{tot}} - nE_{\text{Ta-bulk}}^{\text{tot}} - m\mu_{\text{N}}]/(m+n), \quad (2)$$

where μ_{N} is the (T - and p -dependent) chemical potential of nitrogen. The quantity in Eq. (2) is actually the “grand potential,” where we have neglected vibrational contributions of the bulk systems since p and T effects are much stronger for the gas phase species;²⁰ hence we use the total energies ($T=0$ K) of the respective extended systems in Eq. (2).

The nitrogen chemical potential depends strongly on p and T , where it can be written²⁰

$$\mu_{\text{N}}(T, p_{\text{N}_2}) = 1/2\mu_{\text{N}_2}(T, p_{\text{N}_2}^0) + 1/2kT \ln\left(\frac{p_{\text{N}_2}}{p_{\text{N}_2}^0}\right) + 1/2E_{\text{N}_2}^{\text{tot}}. \quad (3)$$

Here p_{N_2} is the pressure of nitrogen and $p_{\text{N}_2}^0$ corresponds to atmospheric pressure. We choose as the zero reference state of $\mu_{\text{N}}(T, p_{\text{N}_2})$, the total energy of nitrogen in an isolated molecule, i.e., $\mu_{\text{N}}(0 \text{ K}, p_{\text{N}_2}) = 1/2E_{\text{N}_2}^{\text{tot}} \equiv 0$. This will be called

the “nitrogen-rich” condition. The p, T dependence of μ_{N} can be evaluated using tabulated data for $\mu_{\text{N}}(T, p_{\text{N}_2}^0)$.²¹ In general, the typical range of the chemical potential is determined and limited by the pressures and temperatures used in industry and laboratories, namely, from several to thousands of kelvin, and from ultrahigh vacuum ($< 10^{-12}$ atm) to several hundreds of atmospheres.

The value of μ_{N} at which a given tantalum-nitrogen structure becomes *unstable*, i.e., where $E^f(\mu_{\text{N}})=0$, is obtained from rearrangement of Eq. (2) as

$$\mu_{\text{N}} = [E_{\text{defect}}^{\text{tot}} - nE_{\text{Ta-bulk}}^{\text{tot}}]/m, \quad (4)$$

and with respect to the zero reference state of $\mu_{\text{N}}(T, p_{\text{N}_2})$ this becomes

$$\mu_{\text{N}} - 1/2E_{\text{N}_2}^{\text{tot}} = [E_{\text{defect}}^{\text{tot}} - nE_{\text{Ta-bulk}}^{\text{tot}} - m/2E_{\text{N}_2}^{\text{tot}}]/m, \quad (5)$$

which is, by definition, the heat of formation of the Ta-N structure under consideration, per N atom. We refer to this value of μ_{N} as the so-called “N-poor” condition.

Because the total energy of the nitrogen molecule obtained from DFT-LDA (and the generalized gradient approximation) is well known to be significantly overbound, we obtain the total energy of the nitrogen molecule, $E_{\text{N}_2}^{\text{tot}}$, as the difference in total energy of two extended systems, namely, bulk TaN and bulk Ta, together with the experimental value of the heat of formation of TaN. Extended systems are typically described more accurately by DFT compared to free atoms or molecules. The total energy of the nitrogen molecule is therefore obtained by the following equation:

$$1/2E_{\text{N}_2}^{\text{tot}} \approx E_{\text{TaN}}^{\text{tot}} - E_{\text{Ta-bulk}}^{\text{tot}} + \Delta H_f, \quad (6)$$

where $E_{\text{TaN}}^{\text{tot}}$ is the total energy of bulk rocksalt TaN. Here ΔH_f is the experimental heat of formation of TaN in the standard state (room temperature and atmospheric pressure), which is -2.6065 eV.²² The calculated heat of formation of TaN actually agrees quite well with the experimental value but is somewhat underestimated at -2.48 eV.

III. RESULTS

A. Atomic structure

For the “high-concentration” defect structures, as modeled in the “8-atom” cells, we have Ta:N ratios of 2.0, 1.33, 0.75, 0.80, and 0.60 corresponding to two N vacancies, one N vacancy, one Ta vacancy, one N interstitial, and one N antisite (N on a Ta site), respectively. These structures are shown in Fig. 1. The structure containing two N vacancies is just as for Fig. 1(b), but with an additional nearest-neighbor N atom missing. Due to the relatively high defect concentrations, we optimized the equilibrium volume. The vacancy structures are found to have a reduced volume compared to the equivalent (calculated) stoichiometric TaN value: by -1.91% , -0.85% , and -2.55% for the two and one N vacancies and for the Ta vacancy, respectively. The greater contraction for the latter may be anticipated due to the larger size of the missing Ta atom. The N antisite also yields a

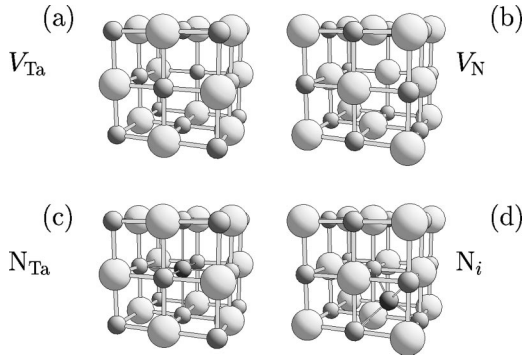


FIG. 1. Atomic geometries of the defect structures: (a) the Ta vacancy V_{Ta} , (b) the N vacancy V_{N} , (c) the N antisite N_{Ta} , and (d) the N interstitial N_i . The large shaded and small dark balls represent Ta and N atoms, respectively.

smaller volume, by -1.52% . The N-interstitial defect induces a larger equilibrium volume than the ideal bulk stoichiometric TaN (by 3.15%) since the lattice expands to accommodate the additional N atom. Due to the high symmetry of these systems, internal relaxations are not possible with the exception of the N interstitial. For the N interstitial and the N antisite, we also consider lower-symmetry geometries which are described below.

The “low-concentration” (“32-atom”) defect systems are calculated using the theoretical bulk TaN lattice constant of 4.37 \AA (the experimental value is 4.385 \AA).²³ The fully relaxed atomic geometry of the defects is described as follows: for the Ta vacancy, the six surrounding, nearest-neighbor N atoms move inwards by about 3% relative to the unrelaxed positions, and for the N vacancy, the six surrounding nearest-neighbor Ta atoms move inwards by $7\% - 10\%$ relative to the unrelaxed positions. Through this latter large relaxation, the Ta atoms approach the Ta-Ta distance that they have in bulk Ta, thus achieving a stronger Ta-Ta bonding; in the ideal rocksalt TaN structure, the Ta-Ta distance is $\approx 8\%$ larger than in bulk Ta (see, e.g., Ref. 23). For the N antisite, the six neighboring N atoms move inwards by a large $8\% - 10\%$ relative to the unrelaxed positions. In each system there are also smaller relaxations of the atoms that are more distant from the defect. The energy gains due to all the atomic relaxations are 0.21 eV and 0.69 eV , respectively, for the Ta and N-vacancy structures. The large value of the latter is mainly due to the large relaxations of the Ta atoms and is similar to the energy loss when expanding bulk bcc Ta by 8% , where the calculated value is 0.56 eV .

The ordered structures Ta_4N_5 and Ta_3N_5 which form in nature are depicted in Figs. 2 and 3. The former has a rock-

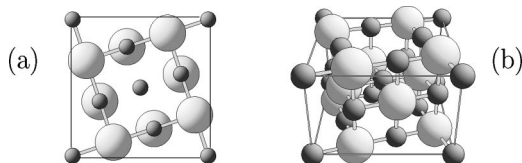


FIG. 2. Structure of Ta_4N_5 : (a) top view and (b) perspective view. The large shaded and small dark balls represent Ta and N atoms, respectively.

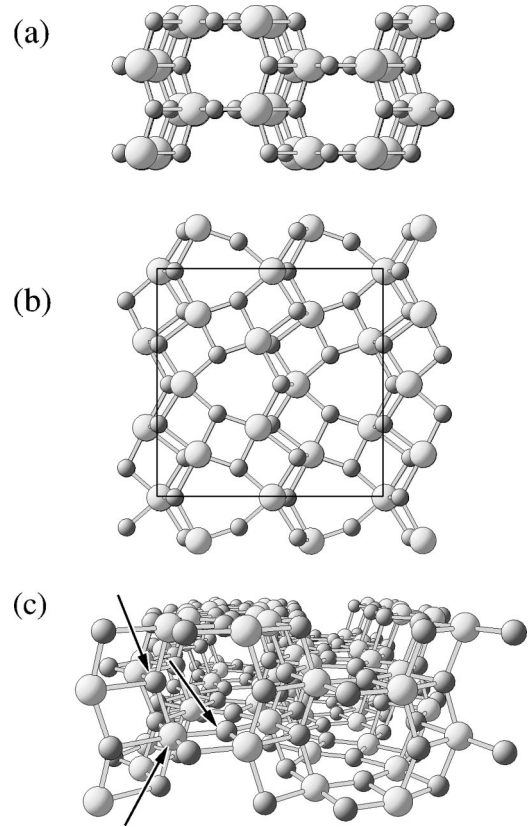


FIG. 3. Structure of Ta_3N_5 : (a) view of the (001) plane, (b) view of the (100) plane where the unit cell is indicated, and (c) perspective view. The large shaded and small dark balls represent Ta and N atoms, respectively. The arrows in (c) indicate the sixfold coordination of the Ta atoms, and the threefold and fourfold coordination of the N atoms.

salt structure and contains an ordered arrangement of Ta vacancies,¹⁰ while the latter (tritanium pentanitride) has the orthorhombic structure, where each Ta atom is surrounded by six N atoms; more specifically, the structure is composed of irregular edge- and corner-sharing TaN_6 octahedra, where the N atoms are threefold and fourfold coordinated.¹¹ The equilibrium volume of Ta_4N_5 is calculated to be 1.81% smaller than the corresponding theoretical bulk TaN volume and is 1.2% smaller than the experimental value. The fully relaxed internal coordinates, given using standard crystallographic notation, are listed in Table I where they are compared to the

TABLE I. Internal atomic coordinates of Ta_4N_5 relative to the unit cell dimensions as obtained by the present calculations (Theory) and experiment (Expt.), Ref. 10, given in standard crystallographic notation. The experimental lattice constants are $a = 6.831 \text{ \AA}$ and $c = 4.269 \text{ \AA}$, and the space group is $I4/m (C_{4h}^5)$.

Atom type	x coordinate		y coordinate		z coordinate	
	Expt.	Theory	Expt.	Theory	Expt.	Theory
8 Ta in $8(h)$	~ 0.2	0.213	~ 0.4	0.396	0.0	0.0
8 N in $8(h)$	~ 0.1	0.092	~ 0.7	0.695	0.0	0.0
2 N in $2(b)$	0.0	0.0	0.0	0.0	0.5	0.5

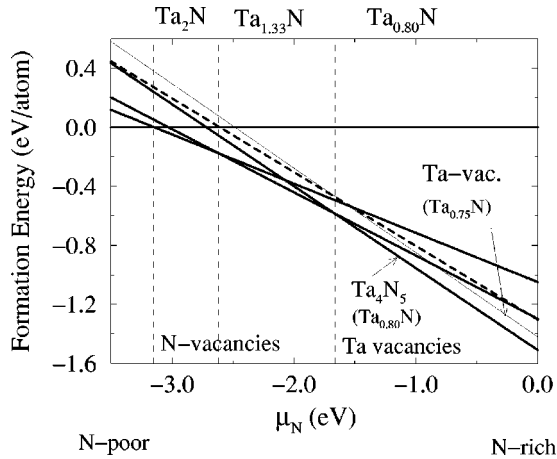


FIG. 4. Formation energies [cf. Eq. (2)] as a function of the nitrogen chemical potential μ_N . The energy for stoichiometric bulk rocksalt TaN is shown as a dashed line. The energy zero of μ_N is taken to be (half) the total energy of the N_2 dimer, which we call the nitrogen-rich condition. The structures listed at the top of the figure indicate the most stable one for the corresponding range of μ_N indicated by vertical dashed lines.

experimental values; excellent agreement can be observed.

For the Ta_3N_5 structure, we optimize the volume of the unit cell, keeping fixed the experimentally determined ratio of the unit vectors (where $a = 3.8862 \text{ \AA}$, $b = 10.2118 \text{ \AA}$, and $c = 10.2624 \text{ \AA}$) as well as the relative positions of the internal coordinates.¹¹ The calculated volume is found to be just 0.1% smaller than experiment.

B. Formation energies

We now turn to consider the formation energies of the various structures. The results for the low-energy structures are displayed in Fig. 4. The lower the energy, the more favorable the system. It can clearly be seen that the energetically most favorable structure for N-rich conditions is the Ta_4N_5 phase ($Ta_{0.8}N$), which is most stable from $\mu_{N_2} = 0$ to -1.65 eV. For lower values of μ_N , namely, from -1.65 to -2.65 eV, the single N vacancy in the 8-atom cell is most stable ($Ta_{1.33}N$), and for still lower values of μ_N , from -2.65 to -3.2 eV, the structure containing *two* N vacancies in the 8-atom cell is most stable (Ta_2N). Interestingly, it can furthermore be observed that stoichiometric TaN (dashed line) is only a *metastable* structure. The next most favorable structures after the Ta_4N_5 phase, in the range $\mu_{N_2} = 0$ to -1.65 eV, are the N and Ta vacancies in the 8-atom cell ($Ta_{1.33}N$ and $Ta_{0.75}N$).

The structures containing the N antisite (not shown) are energetically unfavorable; the values for $\mu_N = 0$ (right side of Fig. 4) are -1.05 eV (-0.49 eV) for the 32- (8-) atom supercells, and they are stable for μ_N down to only -1.98 eV (-0.78 eV). The structures containing N-interstitial atoms (not shown) are even more unfavorable. For the latter two defects, we also investigated the possibility that the N atom may prefer to occupy a lower symmetry site. In particular, for the N interstitial we considered a “split-

interstitial” geometry where two N atoms share a single N-atom site with a N-N distance similar to that in an N_2 molecule. For the N antisite, we considered the possibility that the N antisite moves away from its ideal Ta site towards a neighboring N atom. These geometries, however, had similarly high formation energies.

The structure containing the lower concentration of N vacancies, as calculated in the 32-atom supercell (not shown), is less stable than the one containing the higher concentration (8-atom supercell, $Ta_{1.33}N$) for all ranges of the chemical potential of nitrogen. This can be understood in that on removal of sufficient N atoms, the loss in bonding of neighboring Ta atoms is compensated for by the formation of Ta-Ta metallic bonds. The structure containing the higher concentration of Ta vacancies (8-atom supercell, $Ta_{0.75}N$) is more stable than the one containing the lower concentration (32-atom supercell) (not shown) for strongly N-rich conditions (higher values of μ_N), while for more N-poor conditions (lower values of μ_N), the lower concentration structure is preferred. The latter is, however, notably less favorable than the structures containing N vacancies.

We point out that there is a considerable vacancy-vacancy interaction in these systems so that even with the large 32-atom cells, the energetics obtained may differ from the situation of truly isolated defects. As noted above, the formation energy of Ta_4N_5 is lower than for the other Ta vacancy structures. This is consistent with the fact that Ta_4N_5 represents a phase that is formed in nature. Whether it can actually form under the given experimental conditions in Refs. 2 and 3 will, however, depend on the *kinetics* of the system.

To give some idea of the relationship between the pressure and temperature and μ_N for the present system, we consider the following: For a pressure of 5×10^{-3} Torr (0.66×10^{-5} atm), which is of the order of magnitude used in the experiments,^{2,3} it can be obtained, using Eq. (3), that at temperatures of 300, 600, and 900 K, μ_N takes the values -0.40 , -0.87 , and -1.37 eV, respectively. Inspecting Fig. 4, it can be seen that these values correspond to the region where Ta_4N_5 is most stable. However, if kinetic effects prevent the long-range ordering of this phase, the next most energetically favorable structures are the (“high-concentration”) N and Ta vacancies. In particular, the latter is preferred for smaller absolute values of μ_N (lower temperatures, higher N-pressure) and the former for larger absolute values of μ_N (higher temperatures). Thus, by “togglng” the temperature, the energetically preferred structure can change between these systems. A similar effect occurs for variations in pressure. We propose that this effect is related to the experimentally observed stoichiometry dependence of Ta-N structures on nitrogen pressure and temperature.

C. Electronic structure

Having investigated the atomic structure and energetics of the various systems, we now consider the electronic properties. The total and partial density of states (DOS) of the high-concentration defect systems are shown in Fig. 5. It can be noticed that for the Ta-vacancy [Fig. 5(a)], the N-antisite [Fig. 5(c)], and the N-interstitial [Fig. 5(d)] structures, addi-

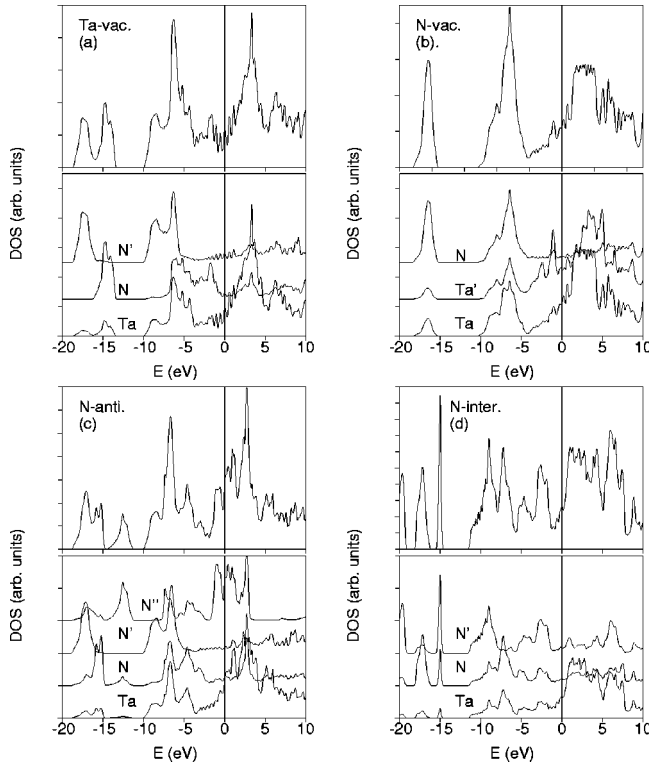


FIG. 5. Total (upper curve in each figure) and partial (lower curves in each figure) density of states for the high-concentration defect structures shown in Fig. 1: (a) the Ta vacancy V_{Ta} , (b) the N vacancy V_{N} , (c) the N antisite N_{Ta} , and (d) the N interstitial N_i . The labeling on the partial DOS means the following: For V_{Ta} , N corresponds to the N atom having 4 Ta neighbors, and that labeled N' , the N atom having 6 Ta neighbors. For V_{N} , Ta corresponds to the Ta atom having 6 N neighbors, and that labeled Ta' ; the Ta atom having 4 N neighbors. For N_{Ta} , the partial DOS labeled by N is for the N atom having 4 Ta and 2 N neighbors, N' is for the N atom having 6 Ta neighbors, and N'' is for the substitutional N atom having 6 N neighbors. For N_i , the partial DOS labeled N corresponds to the atom having 6 Ta neighbors, and that labeled N' , the interstitial atom.

tional states (compared to the single N $2s$ state of bulk TaN at ≈ -16.5 eV) occur in the region -10 to -20 eV. They arise from the N atoms that have a reduced Ta coordination (e.g., the partial DOS of the atom labeled N for the Ta vacancy) or that are bonded to other N atoms (e.g., the partial DOS of the atom labeled N'' for the N antisite). The N vacancy [Fig. 5(b)] and the N antisite [Fig. 5(c)] have a high DOS at the Fermi energy, E_{F} , while the Ta vacancy has a notably *reduced* DOS at E_{F} as compared to bulk TaN [see Fig. 6(a)]. In order to compare the *relative* DOS about the Fermi level for the different structures more quantitatively, we consider the ratio of the integrated total DOS from -0.15 eV up to 0.15 eV to that of the whole valence energy region up to E_{F} . We find that the “low-concentration” Ta-vacancy structure shown in Fig. 6(b) (labeled as $\text{Ta}_{0.94}\text{N}$) has an intermediate DOS at E_{F} (with ratio 0.025) with respect to the stoichiometric TaN (with higher ratio 0.031) and the high-concentration Ta vacancy in Fig. 5(a) (with lower ratio

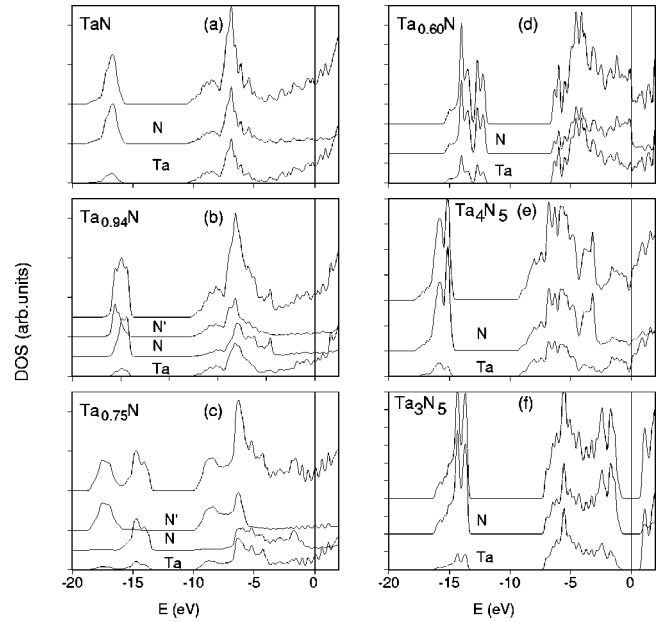


FIG. 6. Density of states (DOS) for (a) bulk TaN, (b) the low-concentration V_{Ta} (calculated in the “32-atom” cell), (c) the high-concentration V_{Ta} (calculated in the “8-atom” cell), (d) an even higher-concentration V_{Ta} (calculated in a cell containing 10 N atoms and 6 Ta atoms), and (e) the Ta_4N_5 and (f) Ta_3N_5 compounds. Total DOS (upper curves), total N and Ta partial DOS (lower curves), as indicated by the labels. N' and N correspond to the partial DOS at the N atom away from and neighboring the Ta vacancy, respectively.

0.020). The DOS of the high-concentration Ta-vacancy system is shown again in Fig. 6(c) (labeled as $\text{Ta}_{0.75}\text{N}$ to indicate the relative ratio of Ta to N atoms). Also shown in Fig. 6(d) is the DOS of a Ta-vacancy system containing an even higher vacancy concentration, namely, $\text{Ta}_{0.6}\text{N}$. This is a defective rocksalt structure calculated in a cell containing 10 N atoms and 6 Ta atoms, i.e., the same cell as for the Ta_4N_5 structure (see Fig. 2), but with an additional Ta vacancy. The relative DOS about E_{F} for this system is higher than for the other structures (ratio 0.032), but it drops sharply above E_{F} . We expect that a lower relative DOS would be found if this structure was calculated in a larger supercell, where additional atomic relaxations could take place. Despite this exception, these results generally show that the presence of Ta vacancies decreases the DOS at and around the Fermi level.

For the Ta-vacancy structures [Figs. 6(b), 6(c), and 6(d)], states in the region -1 to -4 eV below E_{F} can also be seen, where for the “low-concentration” case only a sharp feature around -4 eV occurs. Inspection of the band structure (see below) shows that *defect-related* bands contribute to the DOS in this region, which become narrow for the low-concentration case and give rise to the narrow peak. The Ta-vacancy-induced features are consistent with recent experimental results using x-ray emission spectroscopy⁴ where it is reported that nonbonding N $2p$ -like states form in the energy region between the hybridized Ta- $5d$ -N- $2p$ band and the higher lying Ta- $5d$ band, for the material containing highest Ta vacancies (i.e., $\text{Ta}_{0.85}\text{N}$ in Ref. 4). There is also a

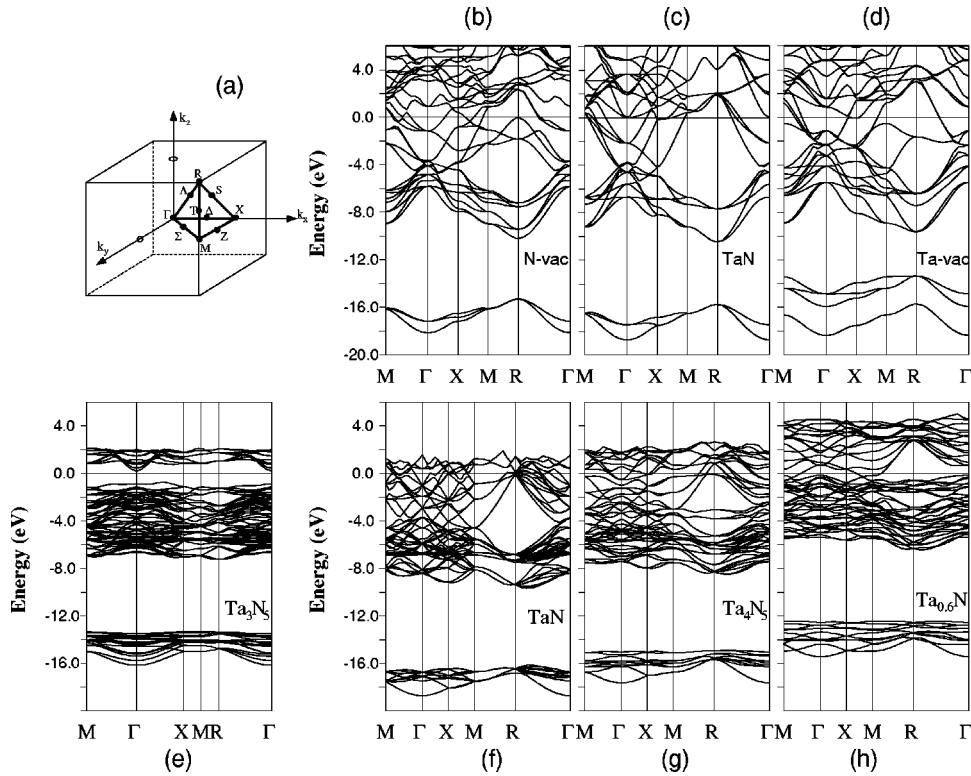


FIG. 7. Upper panel, from left to right: (a) the Brillouin zone indicating the high-symmetry points and lines and the band structure of (b) the N vacancy, (c) ideal bulk TaN, and (d) the Ta vacancy as calculated in “8-atom” cells. Lower panel, from left to right: band structure of (e) the Ta_3N_5 phase, (f) ideal bulk TaN as calculated in a 20-atom cell (for comparison), (g) the Ta_4N_5 phase, and (h) a higher-concentration Ta-vacancy structure $\text{Ta}_{0.6}\text{N}$, calculated in a cell containing 10 N atoms and 6 Ta atoms.

defect-induced band related to the N-2*s* states of the N atoms neighboring the vacancy [see Fig. 7(d)].

The total and partial density of states for the Ta_4N_5 and Ta_3N_5 phases are shown in Figs. 6(e) and 6(f). It can be seen that for the former, the DOS at E_F exhibits a sharp minimum (with ratio 0.016), in contrast to bulk TaN, and there are also new features (compared to bulk TaN) below E_F , at around -3 to -5 eV, as for the high-concentration Ta-vacancy structure described above. There is also an upward shift in the N-2*s* level as seen for the Ta-vacancy systems. For the Ta_3N_5 structure, there is complete filling of the electronic shells and the system exhibits a band gap of 1.5 eV. We note that in reality the band gap will be larger due to the well-known underestimation as obtained when using the LDA. The positions of the N-2*s* states are even higher in energy, which can be correlated with a lower Ta coordination of the N atoms in this system compared to the Ta_4N_5 and Ta-vacancy structures. The insulating nature can be understood from electron counting in that the number of valence electrons in Ta_3N_5 is 40 (3×5 from Ta plus 5×5 from N) and that the *s* and *p* bands of the five nitrogen atoms can accommodate exactly (5×8) 40 electrons.

The band structures for systems containing N- and Ta vacancies, as well as for ideal bulk TaN, are shown in the upper panels (b), (c), and (d) of Fig. 7. For the Ta vacancy, a defect-related state can be seen clearly around -17 eV, as well as new states in the energy range -1 to -4 eV, around the M-R- Γ region. In comparison, the band structure corresponding to the N vacancy exhibits an increased number of bands about E_F as indicated by the higher DOS at E_F mentioned earlier. In the lower panels (e), (f), (g), and (h), the band structure of the Ta_3N_5 phase is shown, as well as that of the ordered Ta-vacancy rocksalt Ta_4N_5 phase. In addition, for

comparison the band structure for ideal stoichiometric TaN is given (calculated in a cell containing 20 atoms to facilitate comparison), as well as that for the highly defective Ta-vacancy structure $\text{Ta}_{0.6}\text{N}$. On going from ideal TaN to Ta_4N_5 to $\text{Ta}_{0.6}\text{N}$, the upward movement and increase in the number of N-2*s* related states can be seen, as well as the appearance of new states in the region -4 to -1 eV [seen at -4.0 to -3.5 in Fig. 7(g) and moving up in energy to -2 to -1 in Fig. 7(h), about the R point].

We note that the present results are based on ground-state electronic structure calculations and do not take into account entropy effects of the extended systems. Furthermore, we have considered only a limited number of the many possible arrangements of the defects. Nevertheless, our results, predicting the formation of Ta-deficient structures (vacancies) for nitrogen-rich material and reduced DOS about E_F and thus reduced conductivity, are all consistent with and help provide an understanding of recent experimental results.

IV. CONCLUSIONS

In summary, we have performed FLAPW calculations to investigate defective TaN structures. Structures containing Ta and N vacancies are found to have the lowest formation energies for N-rich and N-poor conditions, respectively. The presence of Ta vacancies reduces the density of states at E_F by an amount that generally increases with decreasing Ta atom content. This will result in an increased resistivity and a reduction in conductivity compared to stoichiometric TaN. Similarly, the electronic structure of the Ta_4N_5 phase, which forms in nature, exhibits a notable decrease of electronic states at E_F compared to bulk TaN, and for the Ta_3N_5 phase, it is a semiconductor with a (DFT-LDA) band gap of

1.5 eV. Given that in the experiments the systems with dramatically reduced conductivity were prepared for strongly N-rich conditions and *no* new long-range-ordered structures were observed (i.e., in addition to the rocksalt structure), we propose that Ta vacancies and/or regions of Ta-deficient structures are primarily responsible for the metal-to-insulator transition observed experimentally.

ACKNOWLEDGMENTS

This work was supported by the Department of Energy (Grant No. DE-F602-88ER45372) and computing resources provided at NERSC and at the Arctic Region Supercomputing Center. We thank Nate Newman for stimulating discussions.

-
- ¹K. Likharev, Phys. World **10** (5), 39 (1997).
²A. B. Kaul, L. Yu, N. Newman, J. M. Rowell, S. R. Whiteley, and T. Van Duzer, Appl. Phys. Lett. **78**, 99 (2001).
³L. Yu, C. Stampfl, D. Marshall, T. Eshrich, V. Narayanan, J. M. Rowell, N. Newman, and A. J. Freeman, Phys. Rev. B **65**, 245110 (2002).
⁴O. Yu. Khyzhun and Y. V. Zaulchny, Phys. Status Solidi B **207**, 191 (1998).
⁵Y. M. Lu, R. J. Weng, W. S. Hwang, and Y. S. Yang, Thin Solid Films **398**, 356 (2001).
⁶K. Wakasugi, M. Tokunaga, T. Sumita, H. Kubota, M. Nagata, and Y. Honda, Physica B **239**, 29 (1997).
⁷M. H. Tsai, S. C. Sun, C. P. Lee, H. T. Chiu, C. E. Tsai, S. H. Chuang, and S. C. Wu, Thin Solid Films **270**, 531 (1995).
⁸C.-S. Shin, Y.-W. Kim, D. Gall, J. E. Greene, and I. Petrov, Thin Solid Films **402**, 172 (2002).
⁹R. W. G. Wyckoff, *Crystal Structures*, 2nd ed. (Wiley, New York, 1963), Vol. 1, p. 86.
¹⁰*Structure Reports*, edited by W. B. Pearson (Oosthoek, Scheltema, and Holkema, Utrecht, 1969), Vol. 35A, p. 121.
¹¹N. E. Brese, M. O'Keeffe, P. Rauch, and F. J. DiSalvo, Acta Crystallogr., Sect. C **47**, 2291 (1991).
¹²D. S. Yee, J. J. Cuomo, M. A. Frisch, and D. P. E. Smith, J. Vac. Sci. Technol. A **4**, 381 (1986).
¹³K. Schwarz, A. R. Williams, J. J. Cuomo, J. H. E. Harper, and H. T. G. Hentzell, Phys. Rev. B **32**, 8312 (1985).
¹⁴V. A. Gubanov, *Density Functional Theory of Molecules, Clusters and Solids* (Kluwer Academic, Dordrecht, 1995), p. 223.
¹⁵E. Wimmer, H. Krakauer, M. Weinert, and A. J. Freeman, Phys. Rev. B **24**, 864 (1981).
¹⁶A. Canning, W. Mannstadt, and A. J. Freeman, Comput. Phys. Commun. **130**, 233 (2000).
¹⁷L. Hedin and B. I. Lundqvist, J. Phys. C **4**, 2064 (1971).
¹⁸H. J. Monkhorst and J. D. Pack, Phys. Rev. B **13**, 5188 (1976).
¹⁹H. W. Hugosson, P. Korzhavyi, U. Jansson, B. Johansson, and O. Eriksson, Phys. Rev. B **63**, 165116 (2001).
²⁰K. Reuter and M. Scheffler, Phys. Rev. B **65**, 035406 (2002).
²¹D. R. Stull and H. Prophet, *JANAF Thermochemical Tables*, 2nd ed., U.S. National Bureau of Standards (U.S. GPO, Washington, D.C., 1971).
²²*NBS tables of chemical thermodynamic properties: selected values for inorganic and C₁ and C₂ organic substances in SI units*, edited by D. D. Wagman, W. H. Evans, V. B. Parker, R. H. Schumm, I. Halow, S. M. Bailey, K. L. Churney, and R. L. Nuttall [J. Phys. Chem. Ref. Data **11** (Suppl. 2), 2-208 (1982)].
²³C. Stampfl, W. Mannstadt, R. Asahi, and A. J. Freeman, Phys. Rev. B **63**, 155106 (2001).